Acta Oceanol. Sin., 2018, Vol. 37, No. 7, P. 62–68
DOI: 10.1007/s13131-018-1244-y
http://www.hyxb.org.cn
E-mail: hyxbe@263.net

Numerical modeling investigation on turbulent oscillatory flow over a plane rough bed composed by randomly arrayed particles

ZHOU Zhibo[1, 2], ZHANG Jinfeng[1*], ZHANG Qinghe[1], LIU Run[1]

[1] State Key Laboratory of Hydraulic Engineering Simulation and Safety, Tianjin University, Tianjin 300072, China

[2] Center for Ocean Hydrodynamics Research, Tianjin Research Institute for Water Transport Engineering, Ministry of Transport, Tianjin 300456, China

Received 26 August 2017; accepted 10 October 2017

Abstract

A three-dimensional numerical model is established to simulate the turbulent oscillatory boundary layer over a fixed and rough bed composed by randomly arrayed solid spheres based on the lattice Boltzmann method and the large eddy simulation model. The equivalent roughness height, the location of the theoretical bed and the time variation of the friction velocity are investigated using the log-fit method. The time series of turbulent intensity and Reynolds stress are also investigated. The equivalent roughness height of cases with Reynolds numbers of 1×10^4–6×10^4 is approximately 2.81 d (grain size). The time variation of the friction velocity in an oscillatory cycle exhibits sinusoidal-like behavior. The friction factor depends on the relative roughness in the rough turbulent regime, and the pattern of solid particles arrayed as the rough bed in the numerical simulations has no obvious effect on the friction factor.

Key words: turbulence, oscillatory boundary layer, lattice Boltzmann method, large eddy simulations, equivalent roughness height, friction factor

Citation: Zhou Zhibo, Zhang Jinfeng, Zhang Qinghe, Liu Run. 2018. Numerical modeling investigation on turbulent oscillatory flow over a plane rough bed composed by randomly arrayed particles. Acta Oceanologica Sinica, 37(7): 62–68, doi: 10.1007/s13131-018-1244-y

1 Introduction

One of the fundamental problems of coastal engineering is to estimate the oscillatory boundary layer near the seabed, and a better understanding of the wave boundary layer flow over rough beds, including the structure and dynamics of the turbulence and the corresponding bed friction characteristics, is essential to evaluating its effect on sediment transport.

The turbulent oscillatory flow over the rough bed and the bed friction characteristics are the basic topics of sediment transport and wave dissipation (Jonsson, 1966; Swart, 1974; Nielsen, 1992; You and Yin, 2006; Camenen et al., 2009; Ding and Zhang, 2010). Baas et al. (2016) reviewed the bed form and stratification in the field and also examined the extended bed form phase diagram to summarize the bed forms generated in mixtures of sand and mud under rapidly decelerated flows. In addition to observation in the field, experiments on small-scale and large-scale wave flumes have also examined the wave boundary layers over a rough bed (Dixen et al., 2008; Corvaro et al., 2014; Miozzi et al., 2015). Dixen et al. (2008) carried out an experimental investigation on the wave boundary layers over the rough bed composed of ping-pong balls and indicated that the friction factor constantly increased with decreasing the orbital-motion-amplitude-to-roughness ratio a/k_s. Abreu et al. (2013) estimated a new formulation to predict the bed shear stress under the oscillatory flows from oscillating water tunnel experiments. Corvaro et al. (2014) studied the flow dynamics of the oscillatory bottom boundary layer over a permeable bed made of regular plastic spheres and analyzed the features of sweeps and ejections in the surroundings of the bed spheres.

Numerical simulation investigations on the turbulent wave boundary layer as well as the characteristics of the seabed roughness have been carried out. Most of these studies were based on Reynolds-averaged Navier-Stokes (RANS) equations (Puleo et al., 2004; Sana et al., 2009), in which the bed roughness is considered empirically, so that the interaction between the roughness elements and the wave boundary layer cannot be sufficiently represented. Recently, Fornarelli and Vittori (2009) and Ding and Zhang (2010) provided more details on the oscillatory boundary layer over a rough bottom by performing direct numerical simulation (DNS). The rough beds were formed by regularly placed spheres on a plane wall. Although the elements were fully represented with fine grids, the pattern was still different from the plain seabed with sediment particles arrayed randomly. In the present paper, a three-dimensional lattice Boltzmann (LB) model with a large eddy simulation (LES) model was developed to simulate the turbulent oscillatory boundary layer over a rough plane bed consisting of randomly arrayed spheres. The flow statistics as well as the turbulent statistics were obtained. Furthermore, the behaviors of the seabed roughness are investigated and compared with those for a regularly arrayed rough bed.

The rest of the paper is organized as follows: a brief introduction of the LB model is given in section 2; the model setup is introduced in Section 3; Section 4 shows the numerical results; and the conclusions are provided in Section 5.

Foundation item: The National Natural Science Foundation of China under contract No. 51179122; the Science Fund for Creative Research Groups of the National Natural Science Foundation of China under contract No. 51621092.
*Corresponding author, E-mail: jfzhang@tju.edu.cn

2 Lattice Boltzmann method

The LB method aims at modeling fluids in terms of the density distribution function of fictitious particles at the so-called mesoscopic level (Chen and Doolen, 1998). The fundamental concept is to construct simplified kinetic models incorporating mass and momentum conservation principles so that macroscopic averaged properties obey the desired macroscopic equations (Ding and Zhang, 2010). The time evolution of the density distribution function $f_i(\vec{r},\ t)$ in the presence of an external force (e.g., an externally applied pressure gradient) is governed by the discretized Boltzmann equation (Ladd and Verberg, 2001):

$$f_i(\vec{r}+\vec{e}_i\Delta t,\ t+\Delta t) = f_i(\vec{r},\ t) + \Omega_i(f_i) + F_i(\vec{r},\ t), \tag{1}$$

where $\vec{e}_i$ is the discrete velocity vector pointing from node $\vec{r}$ to the adjacent nodes; $\Omega_i(f_i)$ is the collision operator; $F_i(\vec{r},\ t)$ incorporates the effect of external forces; and subscript i represents a discrete direction towards which a particle may move.

A computationally useful form for the collision operator can be constructed by linearizing about the local equilibrium distribution $f_i^{\mathrm{eq}}(\vec{r},\ t)$, i.e.,

$$\Omega_i\left[\vec{f}(\vec{r},\ t)\right] = \sum_j L_{ij}\left[f_j(\vec{r},\ t) - f_j^{\mathrm{eq}}(\vec{r},\ t)\right], \tag{2}$$

where L_{ij} is the matrix elements of the linearized collision operator $\boldsymbol{L}$ (Ladd and Verberg, 2001).

Here, we use the so-called D3Q19 topology, i.e., a three-dimensional cubic lattice with 19 velocity vectors. A suitable form for the equilibrium distribution of the 19-velocity model is

$$f_i^{\mathrm{eq}} = w_i\rho\left[1+\frac{\vec{e}_i\cdot\vec{u}}{c_{\mathrm{s}}^2}+\frac{(\vec{e}_i\cdot\vec{u})^2}{2c_{\mathrm{s}}^4}-\frac{(\vec{u}\cdot\vec{u})}{2c_{\mathrm{s}}^2}\right], \tag{3}$$

where $c_{\mathrm{s}}=\sqrt{c^2/3}$, is the speed of sound, where c is the particle speed, i.e., $c=\Delta x/\Delta t$, in which Δx is the lattice spacing, and the weighting factor w_i is equal to 1/3 (i=0), 1/18 (i=1, 2, ..., 6) and 1/36 (i=7, 8, ..., 18) for the resting particle, six coordinate directions and 12 bi-diagonal directions, respectively.

The hydrodynamic parameters, such as the mass density ρ, the momentum density $\vec{j}$, and the momentum flux $\vec{\Pi}$, are moments of this velocity distribution,

$$\left.\begin{aligned}\rho &= \sum_i f_i\\ \vec{j} &= \rho\vec{u} = \sum_i f_i\vec{e}_i\\ \vec{\Pi} &= \sum_i f_i\vec{e}_i\vec{e}_i\end{aligned}\right\}. \tag{4}$$

The Smagorinsky model is introduced into the LB model to reach high Reynolds numbers. A validate test has been conducted for the oscillatory flow over a rough bed composed of regularly arrayed spheres (Zhou and Zhang, 2016) with the experimental data (Dixen et al., 2008).

3 Simulation setup

The patterns of spheres arrayed in past works were usually regular, and the simulation domain consisted of a few basic rough elements in a hexagonal or cubic pattern. To make a pattern of spheres arrayed on the bottom of the computational domain closer to what is found in nature, the rough bed in the present work was produced by 173 solid spheres of uniform size randomly arrayed in a monolayer (Fig. 1). The distance between any two neighboring spheres was a random value in a range from 0.01 d to 0.10 d, where d is the diameter of a sphere. The purpose was to compare the bed roughness parameters of rough beds arrayed in different patterns. The top of the fluid field was set as a free-slip boundary, the lateral boundaries of the field were set as periodic boundaries, and the bottom of the computational domain and the surface of the spheres were set as bounce-back boundaries. The fluid was driven by an external force.

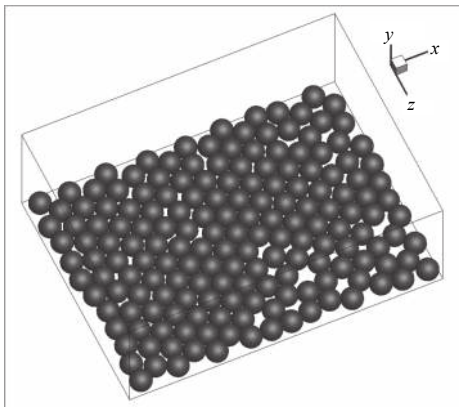

Fig. 1. Computational domain. The rough bed is produced by 173 solid spheres of uniform size randomly arrayed in a monolayer.

The computational domain is 16.2 d×6.0 d×12.2 d (stream-wise direction×vertical direction×span-wise direction). Numerical cases with different a/d and different Reynolds numbers Re_{a} are carried out (Table 1). The values of a/d range from 1.50 to 125, and Re_{a} ranges from 1×10^4 to 6×10^4. Furthermore, a comparable case, C3, with the same Re_{a} as C5 and the same a/d, is also analyzed.

4 Results and analysis

4.1 *Equivalent roughness height*

Ensemble- and space-averaged stream-wise velocity profiles were calculated. Figure 2 shows the velocity distributions at different phases of C2, where 0 in y-axis refers to the crest of spheres. The equivalent roughness height k_{s} and theoretical bed location were obtained via a log-law fit:

$$<\bar{u}>=\frac{u_*}{\kappa}\ln\frac{30y_{\mathrm{t}}}{k_{\mathrm{s}}}, \tag{5}$$

where $<\bar{u}>$ is the ensemble- and space-averaged stream-wise velocity; u_* is the friction velocity; κ=0.4; and y_{t} is the distance to the theoretical bed. The parameters, such as k_{s}, y_{t} and u_*, are calculated by the least squares method.

The phase was taken to be 0 when the flow was in reverse. Figure 3 shows the ensemble- and space-averaged velocity profiles and the log-fit result of case C2 at different phases in semi-logarithmic graphs. The average distance between the theoretical bed and the bottom boundary for the various phases is approximately 0.79 d, with a standard deviation of 0.012. The average equivalent roughness height for the various phases is approxim-

Table 1. Computational parameters for the different cases in the LB model

Case	d^*	U_{*0}	a/d	Re_a	T^*	$L_x^* \times L_y^* \times L_z^*$
C1	36	0.062	1.50	10 000	5 504	580×216×436
C2	24	0.056	5.00	20 000	13 568	388×144×292
C3	20	0.100	11.28	12 300	14 174	324×120×244
C4	20	0.100	13.34	17 200	16 764	324×120×244
C5	20	0.100	25.00	12 300	31 416	324×120×244
C6	20	0.100	25.00	20 000	31 416	324×120×244
C7	20	0.100	50.00	30 000	62 832	324×120×244
C8	20	0.200	125.00	60 000	78 540	324×120×244

Note: d^* is the dimensionless diameter of a sphere, U_{*0} and T^* are the dimensionless maximum free-stream velocity and oscillatory period, respectively, $Re_a=U_o \cdot a/\upsilon$, and $L_x^* \times L_y^* \times L_z^*$ is the dimensionless computational domain.

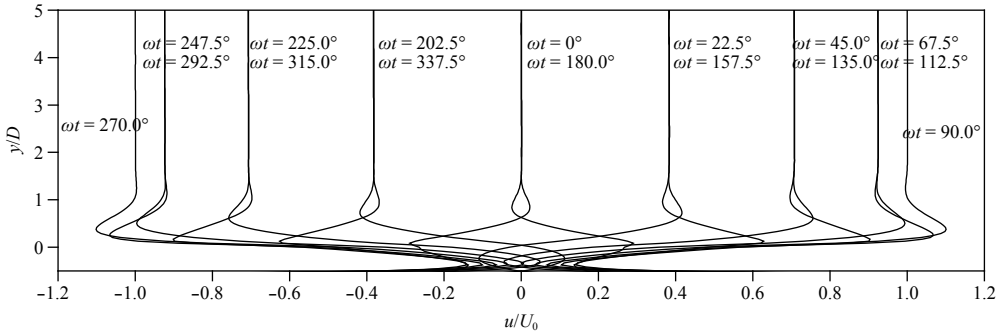

Fig. 2. Velocity distributions of C2 (0 in *y*-axis refers to the crest of spheres).

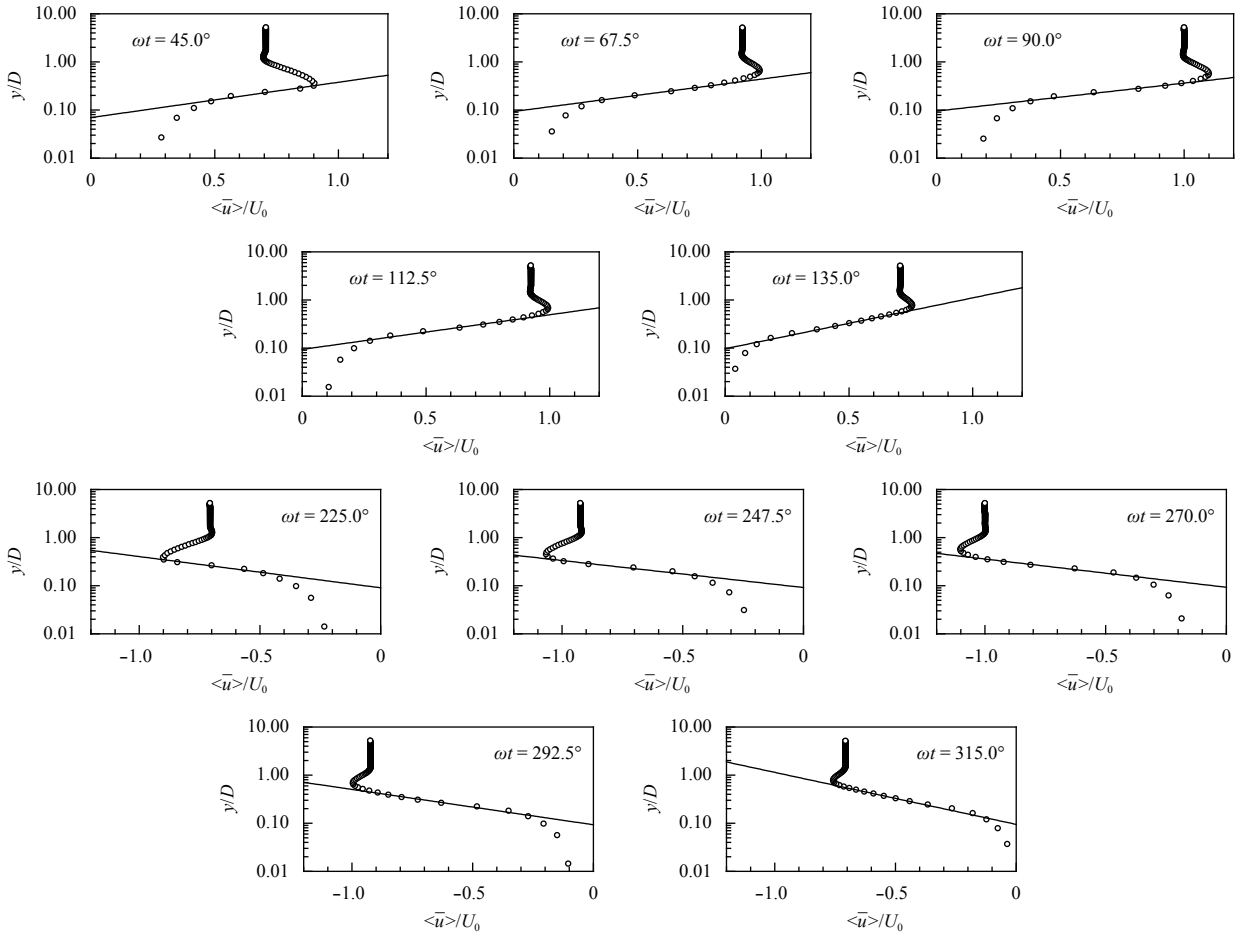

Fig. 3. Ensemble- and space-averaged velocity profiles (circle) and the log-fit results (solid line) at various phases in case C2 (dimensionless with *d*).

ately 2.81 d, with a standard deviation of 0.022. It can be seen that the theoretical bed and the equivalent roughness height have no obvious change with the time phase.

The time-averaged value of the equivalent roughness height k_s^* and the distance between the computational bottom and the location of the theoretical bed y'^* for different cases are shown in Table 2. The distance between the theoretical bed and the bottom is approximately 0.78 d–0.90 d and has an average of 0.81 d. So, the theoretical bed y'^* is located at 0.10 d–0.22 d. Dixen et al. (2008) performed the experiments on the wave boundary layers over beds with roughness elements of stones and ping-pong balls and concluded that y'^* was 0.25 d and 0.23 d, respectively. Ding and Zhang (2010) considered that y'^* was approximately 0.19 d–0.25 d based on the DNS simulation under the oscillatory flow. It can be seen that the present LB simulation shows good agreement with the experimental result by Dixen et al. (2008) and the numerical data by Ding and Zhang (2010).

The equivalent roughness height is in a range of 2.73 d–3.08 d, and the average value of all the cases is 2.81 d, which is close to the recommended value of 2.5 d (Nielsen, 1992) and the experimental results of 2.0 d–2.5 d (Dixen et al., 2008). It is also consistent with the result of approximately 2.8 d obtained from the LB simulation carried out by Ding and Zhang (2010).

From Table 2, we can also see that the equivalent roughness height and the theoretical bed vary little with the Reynolds number Re_a and a/d. During a completely rough turbulent flow, the equivalent roughness height is associated with the particle size of the rough bed, but it has no relation to the amplitude of the orbital motion a and the Reynolds number Re_a.

4.2 *Friction velocity*

The time variation of the friction velocity was also obtained from the log-fitting method (Fig. 4), and it shows a sinusoidal-like behavior. The maximum friction velocity could be obtained from each half-cycle through the sine-fit method for the wave crest u_{*mc} and the wave trough u_{*mc} (Table 3). The maximum friction velocities of two different half-cycles are very close to each other, and is decreasing from C1 to C8 with increasing relevant roughness a/k_s^*.

Table 3 also illustrates the phases of the friction velocities for the wave crest and the wave trough and shows that they lead the free-stream velocity. In laminar flow, the bed shear stress leads the free-stream velocity by 45°. The numerical results here show that the phase lead is in the range between 19.8° and 35.4°. It can be seen that the phase lead is smaller than 45° in smooth and rough turbulent flows (Fig. 5). Other experiments and numerical

Table 2. Average equivalent roughness height k_s^* and the distance between the computational bottom and the location of the theoretical bed y'^* for various cases with different Reynolds numbers

Case	C1	C2	C3	C4	C5	C6	C7	C8	Average
k_s^*	2.81	2.79	3.08	2.73	2.70	2.72	2.80	2.84	2.81
y'^*	0.79	0.82	0.82	0.78	0.79	0.80	0.81	0.90	0.81

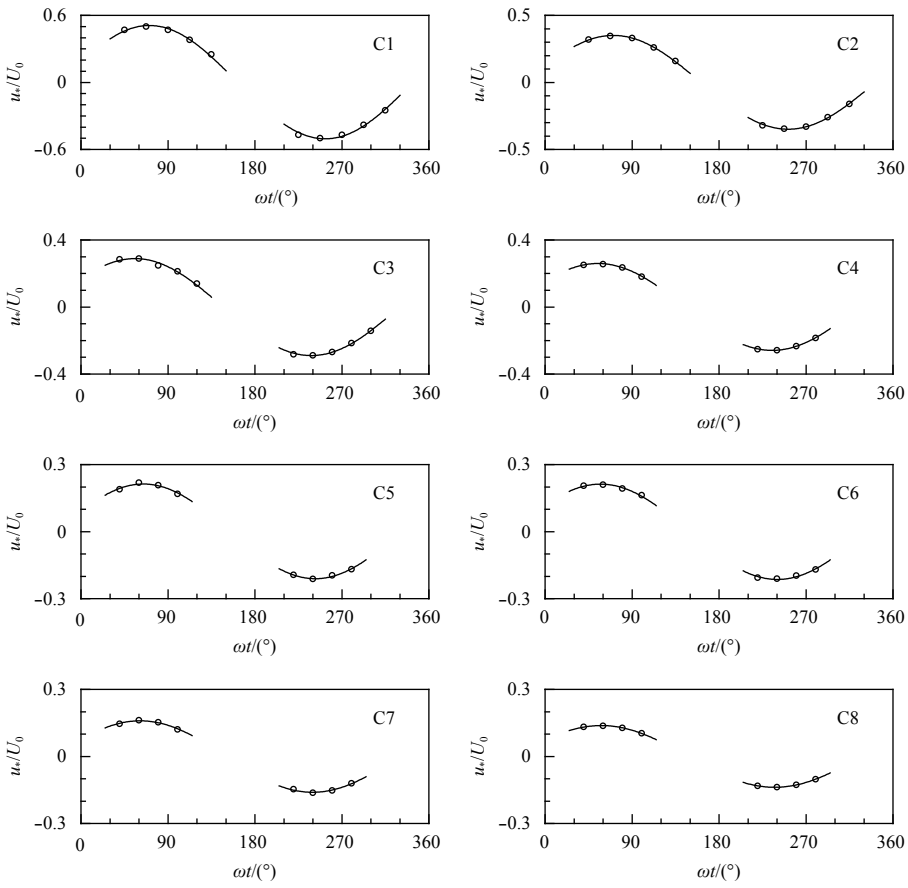

Fig. 4. Time variation of dimensionless friction velocity for various cases.

Table 3. Friction velocities for the crest $u_{*\mathrm{mc}}$ and the trough $u_{*\mathrm{mt}}$, phases for the crest φ_c and the trough φ_t and the phase lead over the free stream velocity $\Delta\varphi$ for various cases with different Reynolds numbers

Case	a/k_s	$u_{*\mathrm{mc}}/U_0$	φ_c/(°)	$u_{*\mathrm{mc}}/U_0$	φ_t/(°)	$\Delta\varphi$/(°)
C1	0.57	0.507	69.7	0.507	249.9	20.2
C2	1.79	0.351	70.1	0.350	250.3	19.8
C3	3.66	0.284	50.6	0.283	230.4	39.5
C4	4.89	0.259	54.7	0.259	235.0	35.2
C5	9.26	0.210	63.8	0.210	241.6	27.3
C6	9.21	0.212	57.3	0.213	240.3	31.2
C7	17.85	0.159	61.3	0.160	239.7	29.5
C8	44.04	0.138	58.1	0.138	237.6	32.2

results, from Jonsson (1966), Sleath (1987), Jensen et al. (1989), Dixen et al. (2008) and Ding and Zhang (2010), are also shown in Fig. 5. It seems that the phase leads have larger values when a/k_s is in the range of 10–100 and relatively small values when a/k_s is smaller than 10 or larger than 100. All of the phase lead results exhibited in Fig. 5 within the range of relevant roughness between 0.46 to 3 683 are smaller than 45°. More experiments or numerical simulations should be carried out with large a/k_s values to provide more data and illustrate the relationship between a/k_s and $\Delta\varphi$ more clearly.

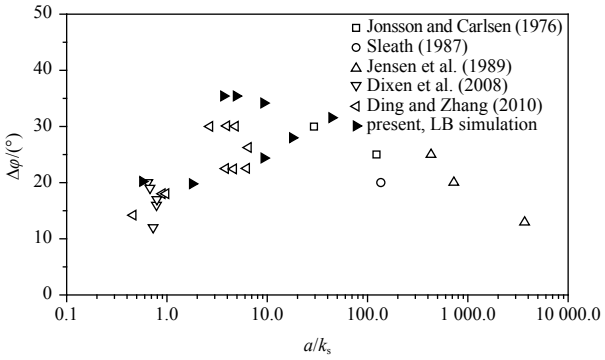

Fig. 5. Phase lead of $u_{*\mathrm{m}}$ over U_0.

4.3 *Friction factor*

The friction factors (Fig. 6) were obtained from the relationship between the friction factor f_w and maximum friction velocity $u_{*\mathrm{m}}$,

$$f_w = 2(u_{*\mathrm{m}}/U_0)^2. \tag{6}$$

The friction factor from the present study is shown as solid cube. Experimental and numerical data from other researchers early to Bagnold and Taylor (1946) are also demonstrated. The friction factor depends on a/k_s and does not vary with the Reynolds number in the rough turbulent regime, which is in good agreement with the conclusion of Jonsson (1966).

The a/k_s values of C1 to C8 are generally in the range of 1–100, and the curve fitting result of C1 to C8 is as follows:

$$f_w = 0.35\left(\frac{a}{k_s}\right)^{-0.63} \quad 0.2 < \frac{a}{k_s} < 100. \tag{7}$$

Some fitting results from Swart (1974), Kamphuis (1975), Soulsby et al. (1993), Simons et al. (2000) and Ding and Zhang (2010) are also plotted in Fig. 6, these curves are generally close

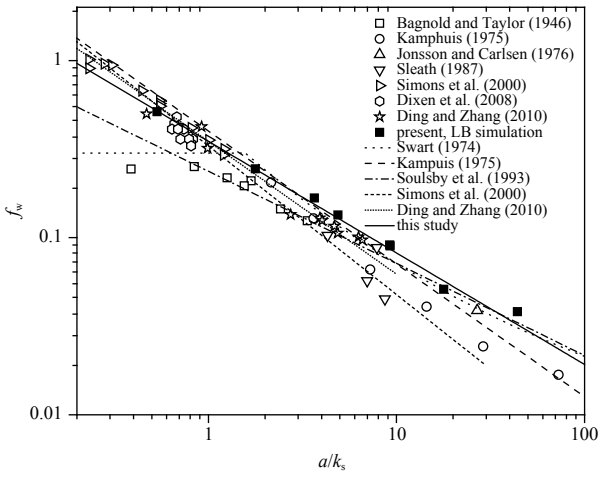

Fig. 6. Relationship between the friction factor f_w and a/k_s.

to each other and agree with the experimental data. Compared with the results obtained from DNS simulations performed by Ding and Zhang (2010), the friction factors of a bed composed of randomly arrayed particles seem to be larger, but by very little, than those of a regular pattern. The friction factor seems to not be sensitive to the patterns of spheres arrayed in numerical simulations.

4.4 *Turbulence characteristics*

The ensemble- and space-averaged turbulent intensity profiles of C2 for different phases of an oscillatory period are displayed in Fig. 7. Here $<\sqrt{u'^2}>/U_0$ and $<\sqrt{v^2}>/U_0$ are the stream-wise component and vertical component of the dimensionless turbulent intensity, respectively. Turbulence is generated near the theoretical bed (y=0 in Fig. 7) after the oscillatory flow reverse (around ωt=22.5° and 202.5°), then transported into the main body of the water by diffusion. The amplitude of the turbulent intensity is increased during the accelerating stage and decreased during the decelerating stage. The development of the turbulent intensity in Fig. 7 reveals the same phenomenon as described in e.g., Sleath (1987), Jensen et al. (1989) and Dixen et al. (2008).

Figure 8 shows the time series of dimensionless ensemble- and space-averaged Reynolds shear stress $<-\overline{u'v'}>/U_0^2$ profiles of C2, where y is the distance from the theoretical bed. The Reynolds stress shows the same development process as the turbulent intensity in Fig. 7. The maximum bed shear stress can be estimated from the amplitude of Reynolds stress profiles (Dixen, 2008). The maximum of the dimensionless bed shear stress

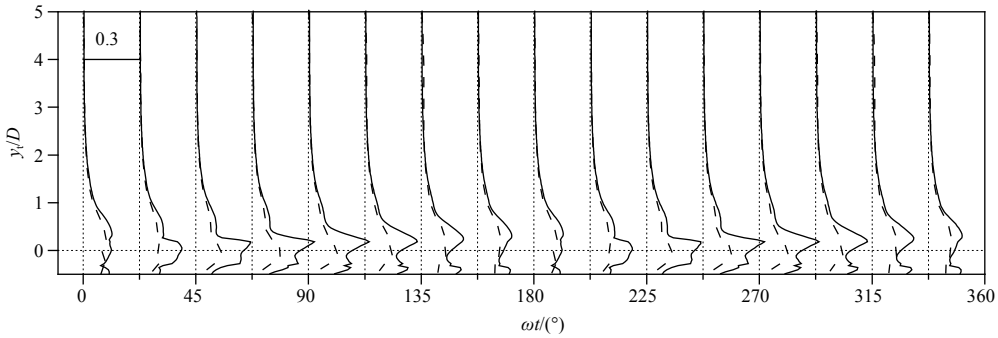

Fig. 7. The turbulent intensity profiles for different phases of an oscillatory period (dimensionless with U_0, line refers to the streamwise component, the dash refers to the vertical component, 0 of y-axis located at the theoretical bed).

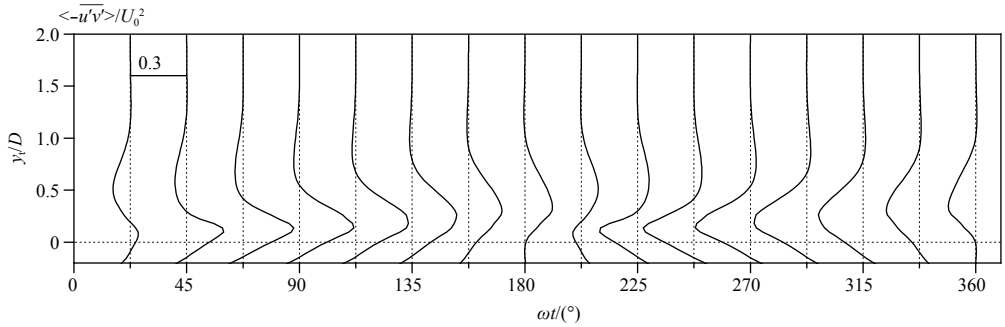

Fig. 8. The Reynolds stress profiles for different phases of an oscillatory period (0 of y-axis located at the theoretical bed).

$\tau_0/\rho U_0^2$ of C2 calculated from Reynolds stress profiles (Fig. 8) is 0.09, slightly smaller than 0.12 which is calculated through the log-law fit method. The same conclusion was reached in Dixen et al. (2008). The reason was ascribed to where the Reynolds stress is the maximum is not precisely at the bed.

5 Conclusions

A rough-bed oscillatory boundary layer composed of randomly arrayed spheres was simulated by a 3-D LB model, and parameters including the equivalent roughness height, the friction velocity and the friction factor were investigated.

The position of the theoretical bed and the equivalent roughness height of the randomly arrayed rough bed obtained using the log-fit method based on least squares seems similar to that of a regularly arrayed bed reported by Ding and Zhang (2010). The theoretical bed is located at 0.10–0.22 times the diameter below the crest of the spheres. The average equivalent roughness height of the cases is 2.81 d, very near the result of 2.8 d obtained by Ding and Zhang (2010), and both values are slightly larger than the recommended value of 2.5 d.

The time variation of the friction velocity in an oscillatory cycle obtained by the log-law fit method exhibits a sinusoidal-like behavior. The phase leads of the friction velocity over the free stream velocity are in the range of 27°–40° for the relative roughness values a/k_s =3.66–44.04. A curve fitting equation of the friction factor for a/k_s in the range of 1–100 was obtained from the simulation results. The friction factor is not sensitive to the pattern of the spheres in the numerical simulations.

The time series of the turbulent intensity and the Reynolds stress are also investigated. Turbulence is generated near the theoretical bed after the oscillatory flow reverse and transported into the main body of the water by the diffusion. The bed shear stress determined from the Reynolds-stress is slightly smaller than that from the log-law fit method.

It should be noted that the results of the present paper, based on the simulation of single layer particles, consider no percolation of multilayer noncohesive sand particles. Therefore, future investigation with the effect of percolation is needed, which can be applied into a real sandy coast.

References

Abreu T, Michallet H, Silva P A, et al. 2013. Bed shear stress under skewed and asymmetric oscillatory flows. Coastal Engineering, 73: 1–10

Baas J H, Best J L, Peakall J. 2016. Predicting bedforms and primary current stratification in cohesive mixtures of mud and sand. Journal of the Geological Society, 173(1): 12–45

Bagnold R A, Taylor G. 1946. Motion of waves in shallow water. Interaction between waves and sand bottoms. Proceedings of the Royal Society: A. Mathematical, Physical, and Engineering Sciences, 187(1008): 1–18

Camenen B, Larson M, Bayram A. 2009. Equivalent roughness height for plane bed under oscillatory flow. Estuarine, Coastal and Shelf Science, 81(3): 409–422

Chen S, Doolen G D. 1998. Lattice Boltzmann method for fluid flows. Annual Review of Fluid Mechanics, 30(1): 329–364

Corvaro S, Miozzi M, Postacchini M, et al. 2014. Fluid-particle interaction and generation of coherent structures over permeable beds: an experimental analysis. Advances in Water Resources, 72: 97–109

Ding Lei, Zhang Qinghe. 2010. Lattice Boltzmann simulation to characterize roughness effects of oscillatory boundary layer flow over a rough bed. In: Smith J M, Lynett P, eds. Proceedings of the 32nd Conference on Coastal Engineering. Shanghai: Coastal Engineering Research Council, 1397–1407

Dixen M, Hatipoglu F, Sumer B M, et al. 2008. Wave boundary layer over a stone-covered bed. Coastal Engineering, 55(1): 1–20

Fornarelli F, Vittori G. 2009. Oscillatory boundary layer close to a rough wall. European Journal of Mechanics - B/Fluids, 28(2): 283–295

Jensen B L, Sumer B M, Fredsøe J. 1989. Turbulent oscillatory boundary layers at high Reynolds numbers. Journal of Fluid Mechanics, 206: 265–297

Jonsson I G. 1966. Wave boundary layers and friction factors. In: O'Brien M P, ed. Proceedings of the 10th International Conference on Coastal Engineering. Tokyo: ASCE, 127–148

Jonsson I G, Carlsen N A. 1976. Experimental and theoretical investigations in an oscillatory turbulent boundary layer. Journal of Hydraulic Research, 14(1): 45–60

Kamphuis J W. 1975. Friction factor under oscillatory waves. Journal of the Waterways, Harbors and Coastal Engineering Division, 101(2): 135–144

Ladd A J C, Verberg R. 2001. Lattice-Boltzmann simulations of particle-fluid suspensions. Journal of Statistical Physics, 104(5-6): 1191–1251

Miozzi M, Postacchini M, Corvaro S, et al. 2015. Whole-wavelength description of a wave boundary layer over permeable wall. Experiments in Fluids, 56(6): 127

Nielsen P. 1992. Coastal Bottom Boundary Layers and Sediment Transport. Singapore: World Scientific Publishing Company, 102–109

Puleo J A, Mouraenko O, Hanes D M. 2004. One-dimensional wave bottom boundary layer model comparison: specific eddy viscosity and turbulence closure models. Journal of Waterway, Port, Coastal and Ocean Engineering, 130(6): 322–325

Sana A, Ghumman A R, Tanaka H. 2009. Modeling of a rough-wall oscillatory boundary layer using two-equation turbulence models. Journal of Hydraulic Engineering, 135(1): 60–65

Simons R, Myrhaug D, Thais L, et al. 2000. Bed friction in combined wave-current flows. In: Edge B L, ed. Proceedings of the 27th International Conference on Coastal Engineering. Sydney: ASCE, 216–226

Sleath J F A. 1987. Turbulent oscillatory flow over rough beds. Journal of Fluid Mechanics, 182: 369–409

Soulsby R L, Hamm L, Klopman G, et al. 1993. Wave-current interaction within and outside the bottom boundary layer. Coastal Engineering, 21(1–3): 41–69

Swart D H. 1974. Offshore sediment transport and equilibrium beach profiles [dissertation]. Delft: Delft University of Technology

You Zaijin, Yin Baoshu. 2006. A unified criterion for initiation of sediment motion and inception of sheet flow under water waves. Sedimentology, 53(5): 1181–1190

Zhou Zhibo, Zhang Qinghe. 2016. 3-D lattice Boltzmann simulation of turbulent oscillatory boundary layer flow over rough beds. Journal of Hydrodynamics (in Chinese), 31(4): 463–471